EASR

Engineering and Applied Science Research

https://www.tci-thaijo.org/index.php/easr/index

Published by the Faculty of Engineering, Khon Kaen University, Thailand

Creep behaviors of ASTM A36 welded joints

Pavaret Preedawiphat[1)], Numpon Mahayotsanun*[1)], Keerati Sa-ngoen[2)], Mai Noipitak[3)], Pongsak Tuengsook[4)], Sedthawatt Sucharitpwatskul[5)] and Kuniaki Dohda[6)]

[1)]Department of Mechanical Engineering, Faculty of Engineering, Khon Kaen University, Khon Kaen 40002, Thailand
[2)]LPN Metallurgical Research Center (LPNMRC), Samutprakarn 10290, Thailand
[3)]Materials and Nondestructive Testing Laboratory, Ratchaburi Learning Park, Office of the President, King Mongkut's University of Technology Thonburi, Bangkok 10140, Thailand
[4)]Department of Production Engineering, Faculty of Engineering, King Mongkut's University of Technology Thonburi, Bangkok 10140, Thailand
[5)]National Metal and Materials Technology Center (MTEC), National Science and Technology Development Agency (NSTDA), Pathum Thani 12120, Thailand
[6)]Department of Mechanical Engineering, Northwestern University, Evanston, Illinois, 60208, USA

Received 4 October 2020
Revised 27 December 2020
Accepted 18 January 2021

Abstract

This research work aimed to observe the creep behaviors of the ASTM A36 welded joints. The microstructure and hardness of the base zone (BZ), heat affected zone (HAZ), and weld fusion zone (WFZ) were measured. Afterward, the residual stresses on the welded plate were observed to determine any lead to fatigue failure. The hot tensile tests were then performed to investigate the welded specimens' creep behaviors at varied strain rates and temperatures. The power-law model was applied to describe the creep behaviors at each testing condition. Finally, the scanning electron microscopic (SEM) images of the tested specimens were observed to identify breakage causes. The creep results showed that the weakest locations were found in the base (A36) zones. The areas prone to ductile fracture was the base zones close to HAZ.

Keywords: ASTM A36, Creep, Hot tensile test, Weld

1. Introduction

Welded steel pipes used in thermal, chemical, petroleum, and nuclear power plants are typically exposed to high stress and temperatures. Even though these welded pipes were designed to meet the maximum allowable primary stress, they were not guaranteed to reduce creep failure risks during the boiler service life [1]. As a result, creep life estimations and inspection plans must be revised. The creep behaviors could be observed by measuring the strain under fixed stress at an elevated temperature over time [2]. The underlying creep mechanisms observed during the tests would help identify the creep failures' potential root causes [3]. Recently, creep-resistant steels have been developed and enhanced to operate at higher temperatures at longer service life [4]. Much attention has also been paid to the welded joints because degradations and fractures could be developed [5]. The effects of heating, filler material, heat affected zone (HAZ) formation during the welding processes and post-weld heat treatments (PWHT) could influence the creep behaviors and creep life of the welded joints [6]. Pandey et al. explored the effects of PWHT and re-austenitization (normalizing) followed by tempering treatment (PWNT) on the welded P91 welded joints, and the PWNT resulted in the homogeneous microstructure formation across the welded joint [7]. Pandey et al. also found out that the Type-IV mode of failure occurred in the FGHAZ and inter-critical heat affected zone (ICHAZ) [8]. The microstructure evolution of creep rupture was commonly assessed [9]. The review of the microstructure evolution in the P91 welds in different conditions was summarized by Panday et al. [10].

Creep fractures could be reduced by avoiding the probability of crack initiation and growth in the welded joints [11]. Zhao et al. studied the creep damage evolution of ASME 92 welded joints and found out that the most severe location was in the fine-grained heat-affected zone (FGHAZ) [12]. The lower creep rupture life with decreased rupture ductility found in the welded joint was observed by Sakthivel et al. [13]. Wei et al. 's research work showed that the stress influenced the growth of the micro-cavities and crack formation, which led to the creep rupture [14]. Liu et al. identified the particular zone in multi-layer and multi-pass welded metal and observed that the primary rupture mechanism resulted from the grain boundary failure at high temperature [15]. El-Desoky noticed that the softer martensite matrix acceleration affecting the welded joints' creep rupture strength was influenced by the more refined austenite grains [16].

Residual stresses could be measured to determine the degree of damages caused by uneven plastic strains on welded joints [17]. Taraphdar et al. developed a novel technique called deep hole contour (DHC) to evaluate through-thickness residual stress fields with

*Corresponding author. Tel.: +666 3789 2914
Email address: numpon@kku.ac.th
doi: 10.14456/easr.2021.47

a low degree of damage to the specimen [18]. The numerical thermal analysis could also be performed to investigate the effects of heat input and residual stress on welded joints [19].

Various constitutive equations and creep damage mechanics have been developed to understand creep mechanisms [20]. Different creep models based on plasticity theories have been commonly applied to describe creep behaviors [21]. In welded joints, the numerical investigation could be applied to determine maximum principal stress locations; thus, the Type-IV cracking could be suppressed [22]. The observation of plastic strains at elevated temperatures could also be numerically simulated to describe the fracture locations [23]. The creep-life assessments of welded joints are necessary to avoid creep failure during the service and help predict the lifetime of welded joints [24-30].

The welded joints of ASTM A36 steel have still been used in some power plants, but the creep behaviors and causes of failure of these welded joints are still unknown. This paper aimed to understand the creep behaviors of ASTM A36 welded joints and analyze the potential cause of creep failure. The welded joints were optically observed, the hardness values were measured, and the residual stress was evaluated. Then, the creep tests under different strain rates and temperatures were carried out. Also, optical microscopic examinations were conducted to understand the rupture mechanisms. Finally, the creep failure mode was determined to utilize the welded joints appropriately.

2. Materials and methods

2.1 Welded specimens preparation

Before the welding process, two ASTM A36 steel plates were preheated at 150°C. These ASTM A36 plates were then welded by Gas Tungsten Arc Welding (GTAW) in the first two layers. Subsequently, layers three to thirteen were welded by Shielded Metal Arc Welding (SMAW). Table 1 presents the welding process parameters for the welded specimens preparation.

The shielding gas of 99.9% argon with a 10-15 liter/minute flow rate was used in GTAW. In the SMAW process, the weld groove angle was 60° with the root height and root gap at 3 mm, as shown in Figure 1. The chemical compositions of both joint and filler materials are reported in Table 2. Table 3 provides the mechanical properties of these materials.

Table 1 Welding process parameters for the welded specimens preparation

Welding process	Layers	Filler metals	Filler diameter (mm)	Current type and polarity	Current (Amp)	Voltage (V)	Travel speed (mm/min)
GTAW	1 - 2	ER70S-6	2.4	DCEN	90 - 140	10 - 15	50 - 100
SMAW	3 - 13	E7016	3.2	DECP, AC	90 - 130	22 - 30	60 - 120

Table 2 Chemical compositions of the filler and joint materials

Materials	C	Mn	Cr	Si	Mo	Ni	Cu	S	P
ER70S-6	0.100	1.560	0.020	0.860	< 0.010	0.010	0.240	0.012	0.012
E7016	0.080	0.940	0.020	0.600	< 0.100	0.010	-	0.006	0.004
ASTM A36	0.250 (maximum)	0.850 - 1.350	-	0.400 (maximum)	-	-	-	0.030	0.030

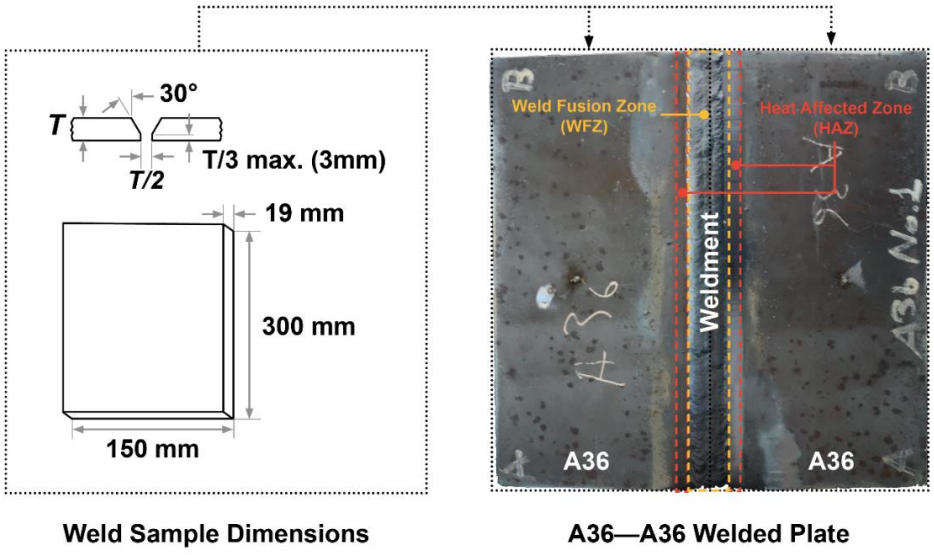

Figure 1 A36-A36 welded plate.

Table 3 Mechanical properties of the filler and joint materials

Materials	Yield Strength (N/mm^2)	Tensile Strength (N/mm^2)	Elongation (%)
ER70S-6	420	550	35
E7016	420	520	33
ASTM A36	250	400 - 550	23

The post-weld heat treatment (PWHT) was carried out at 595°C to 630°C for an hour with the maximum heating and cooling rate of 200°C/hour. Afterward, the welded joint's cross-section was observed to evaluate the weldment quality, as illustrated in Figure 2.

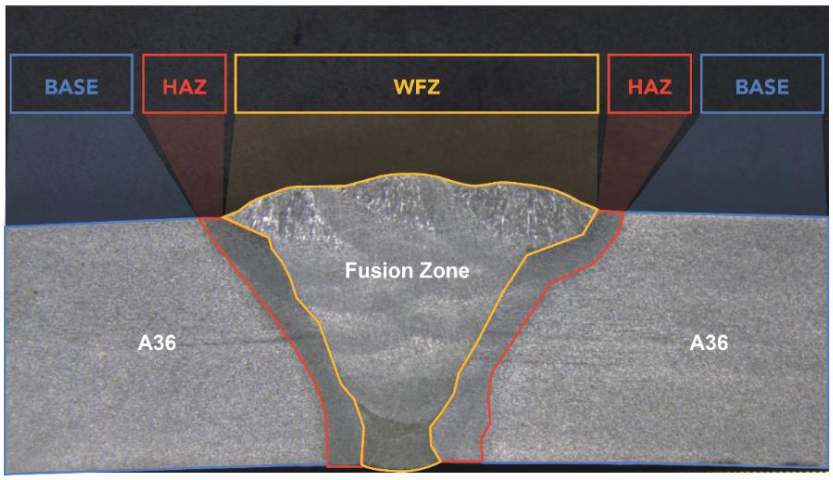

Figure 2 Cross-section of the A36-A36 weldment.

2.2 Hardness tests

Three major zones could be distinguished in the welded joint: base zone (BZ), heat affected zone (HAZ), and weld fusion zone (WFZ), as presented in Figure 3. The Vickers hardness test was carried out to observe each zone's material strengths by measuring the hardness values at the specified measurement locations. All of the hardness measurements were performed by using the Mitutoyo HV-115 hardness testing machine. In each hardness test, the pyramid diamond indentor having a 136° angle was applied with 10 kgf load for the dwell time of 15 s.

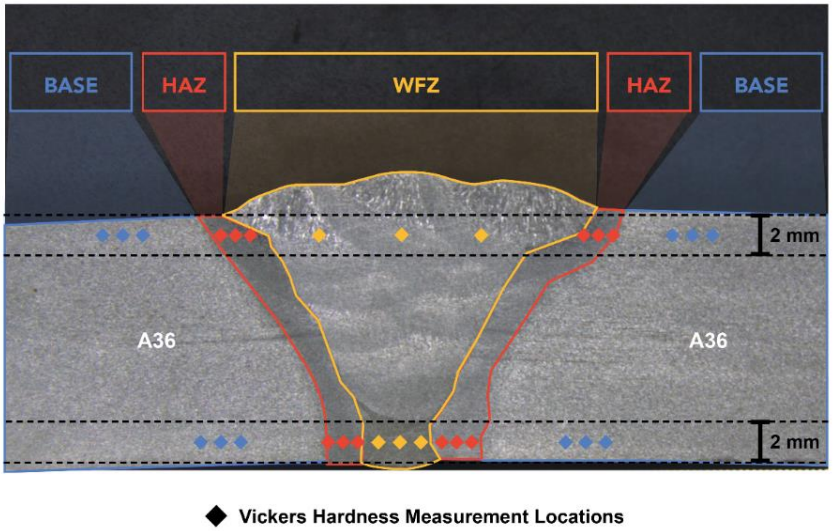

Figure 3 Hardness measurement locations.

2.3 Residual stress tests

There are internal stresses in welded joints due to heating and cooling in the welding process. Thus, residual stress should be evaluated to ensure that internal stress distortions are not too large. In this study, PULSTEC μ-X360s Portable X-ray Residual Stress Analyzer was used to measure the welded plate's residual stress. The measurement locations (B1 to B9) covered the areas of BZ, HAZ, and WMZ, as indicated in Figure 4.

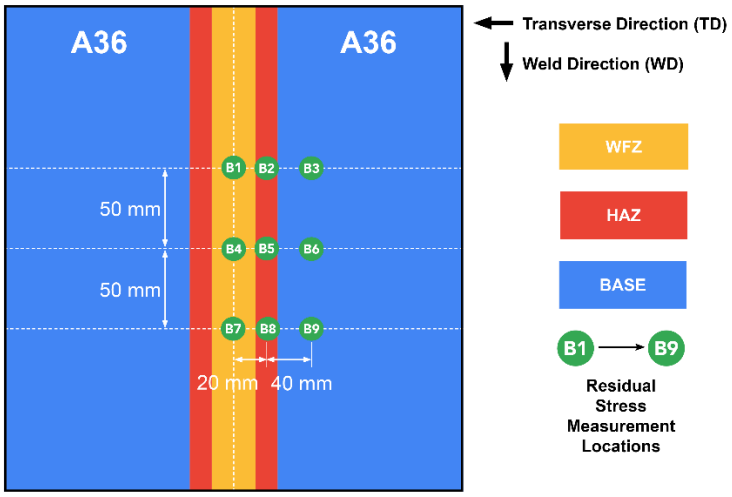

Figure 4 Residual stress measurement locations.

2.4 Creep tests

The welded ASTM A36 plate's creep behaviors were observed by carrying out the hot tensile tests following the ASTM E8 standard. The following creep specimens were considered: base specimen (A36) and welded specimen (A36-A36). These specimens were cut from the specified locations in Figure 5, machined to be rod shapes with 8 mm diameter and 52 mm gauge length. The hot tensile tests were performed by using the Instron 1000 HDX, as displayed in Figure 6.

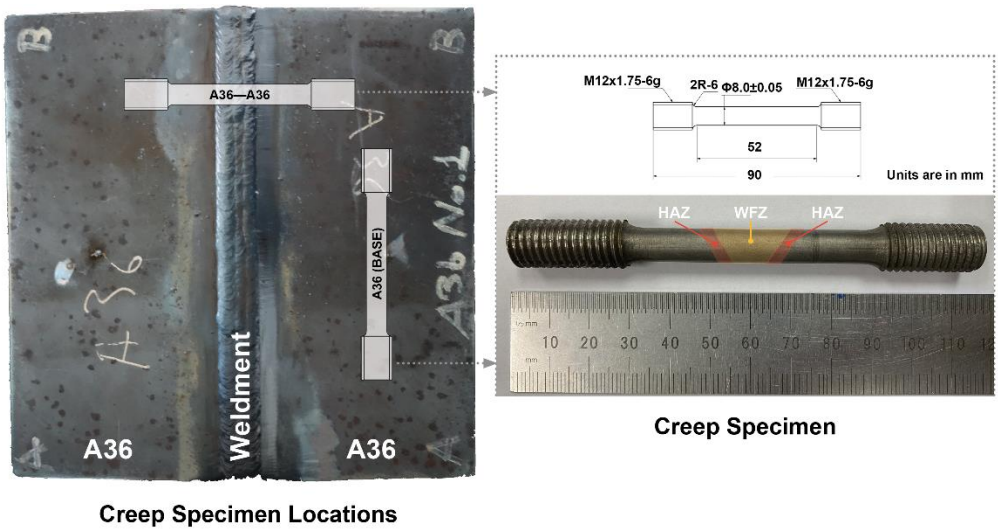

Figure 5 Creep specimens.

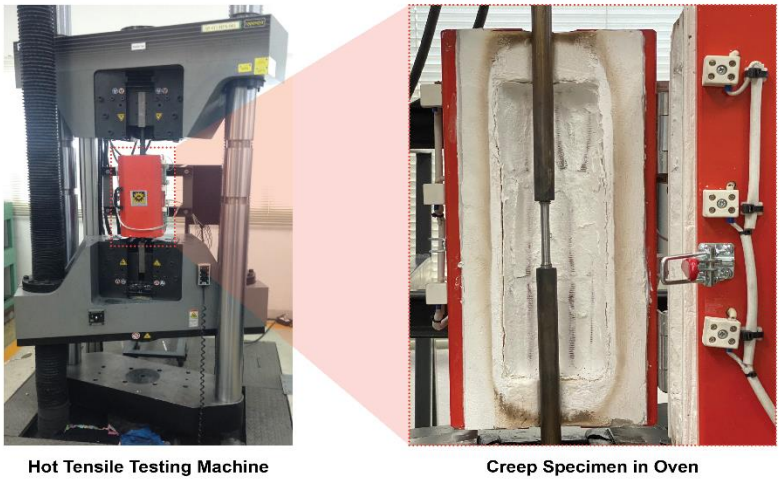

Figure 6 Set creep specimen in the oven of the hot tensile testing machine.

In each test, the creep specimen was located in the oven and set under certain temperatures and strain rates until breakage. All the testing conditions of the creep tests investigated in this study are presented in Table 4. Each test's load, strain, and temperature data were recorded and post-processed to develop the stress-strain curves for creep behavior evaluation.

Table 4 Creep testing conditions

Specimens	Strain Rates (s^{-1})	Temperature (°C)
A36	0.002, 0.010, 0.020	500, 550, 600, 650
A36-A36	0.010, 0.020, 0.030	500, 550, 600

3. Results

3.1 Microstructures

The optical microscopic images of the cross-section surface area of the A36-A36 weldment are presented in Figures 7 and 8. The overall structure of BZ, HAZ, and WFZ consisted of ferrite (light areas) and pearlite (dark areas). In the BZ, the banded structure of ferrite and pearlite originated from the hot rolling process. The coarse-grained (CG) areas could be observed in the BZ located further away from the WFZ. A similar structure could be seen in the BZ close to HAZ but with smaller grains due to pearlite decomposition influenced by the heat during the welding process and PWHT. Particularly at HAZ, the fine-grained (FG) areas were mainly apparent. Since the welded materials were ASTM A36, the WFZ was considered homogeneous, consisting of carbide and ferrite. The amount of pearlite in the WFZ was much less than those of the HAZ and BZ because the amount of percentage of carbon composition was much higher (Table 2). The grains in the WFZ were smaller than those of the FG areas in HAZ. Note that the shapes of the grains in the WFZ were equiaxed (carbide around ferrite grains).

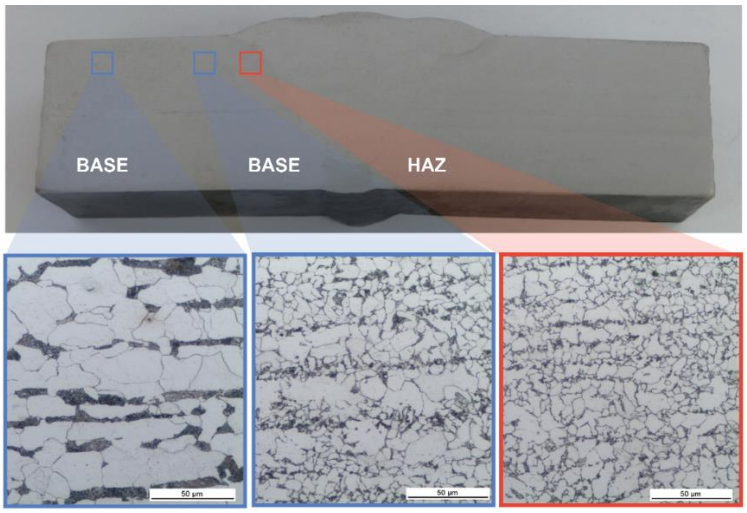

Figure 7 Microstructures of the A36-A36 weldment (BZ and HAZ locations).

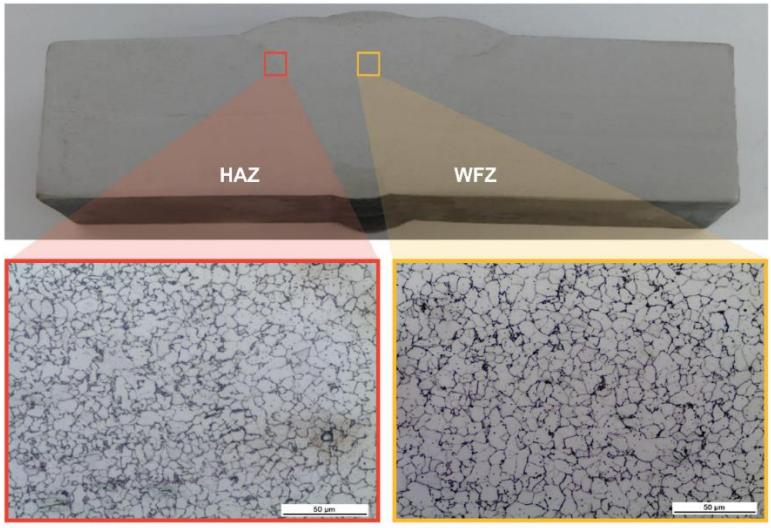

Figure 8 Microstructures of the A36-A36 weldment (HAZ and WFZ locations).

3.2 Hardness results

Figure 9 shows the Vicker hardness measurement results of the A36-A36 weldment. The top and bottom graphs were the hardness results of the top and bottom lines shown on the left (measured positions). This variation in hardness results was commonly presented to determine the soft and hard areas in different zones [31, 32]. Based on the top and bottom graphs in Figure 9, the highest to lowest hardness values ranged from the WFZ to HAZ, to the BZ, respectively. The locations having higher hardness values offered higher strengths, which also correspond to the smaller grain areas. As a result, the effects of different grain size and hardness directly led to the various mechanical properties in these three zones. The distortions on both sides of the BZ were the distinct indicator of the affected mechanical properties.

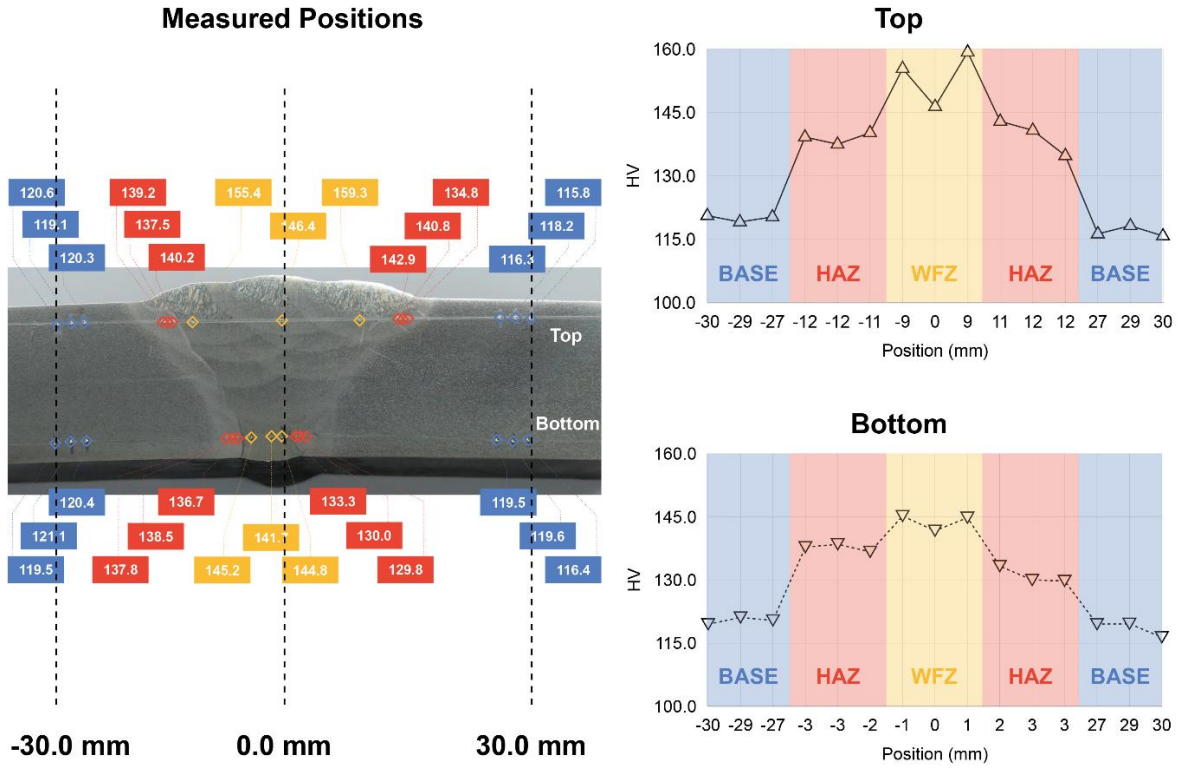

Figure 9 Hardness results of the A36-A36 weldment.

3.3 Residual stress results

The in-plane principal stresses were measured by the x-ray diffraction method in the Transverse Direction (TD) and Weld Direction (WD), as illustrated in Figure 10. The positive values indicated tensile stresses, while the compressive stresses were negative values. These stresses resulted from the heating and cooling of the welded plate during the welding process. It could be observed that the high compressive stresses were found in the WFZ and HAZ towards the middle area of the plate. Despite the variations in the measured stress results in different locations, these differences did not lead to high distortions and influence fatigue failure. As a result, the residual stresses found in the A36-A36 welded plate was considered acceptable.

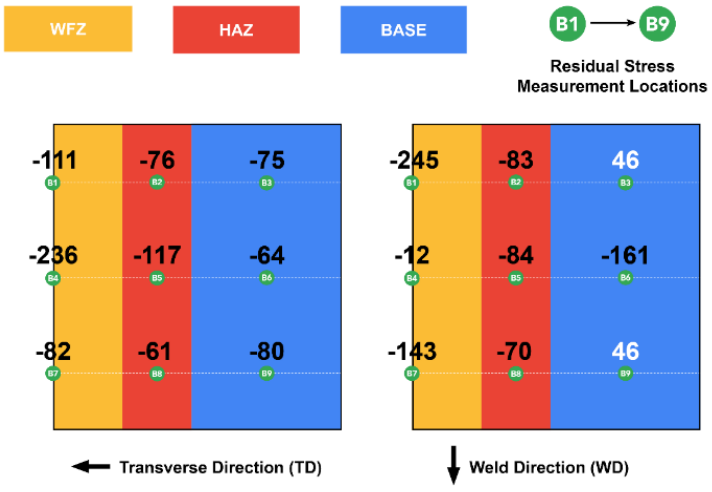

Figure 10 Residual stress results of the A36-A36 welded plate.

3.4 Creep test results

The creep testing results of A36-A36 welded plate can be observed through the true stress - true strain curves of the hot tensile tests, as presented in Figures 11 and 12. The graphical results in the top row show the true stress - true strain results at different temperatures. Also, the strain rates increase from left to right column. In the bottom row, the log-log plots of the true stress - true strain curves are illustrated.

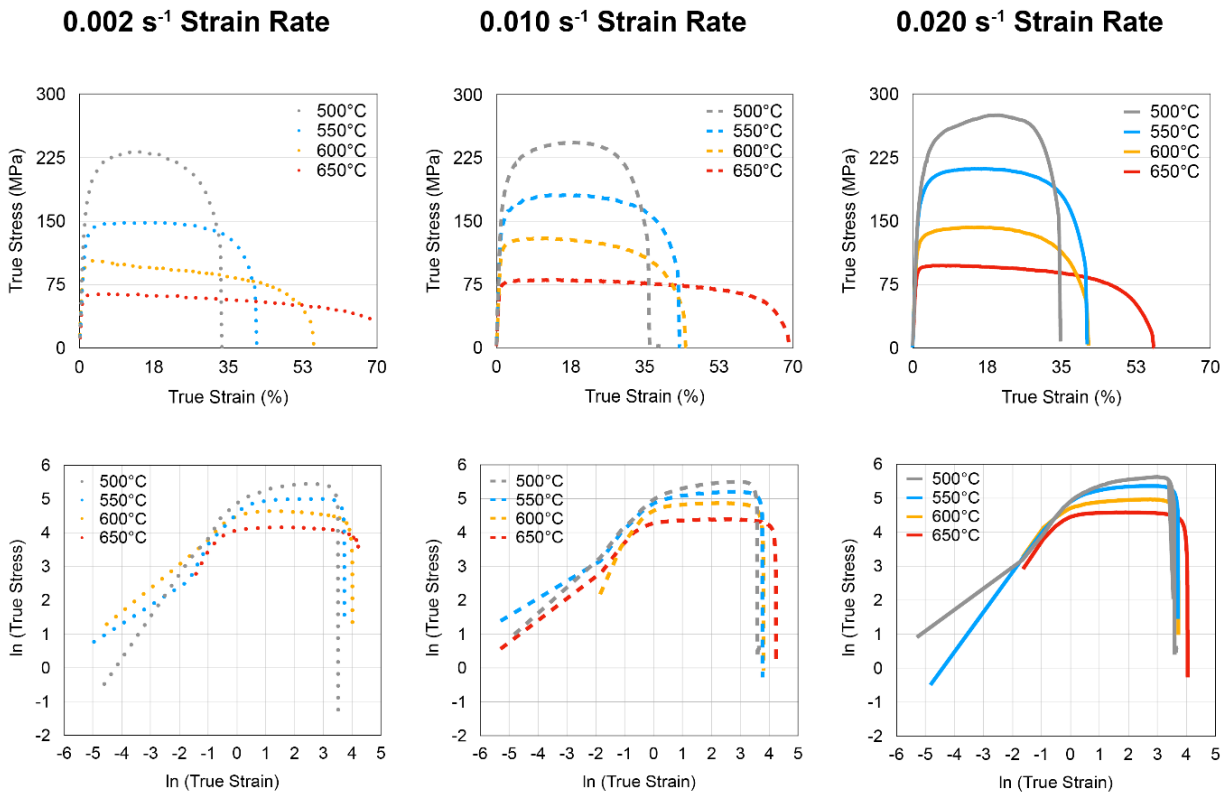

Figure 11 Hot tensile testing results of the A36 (Base) specimens.

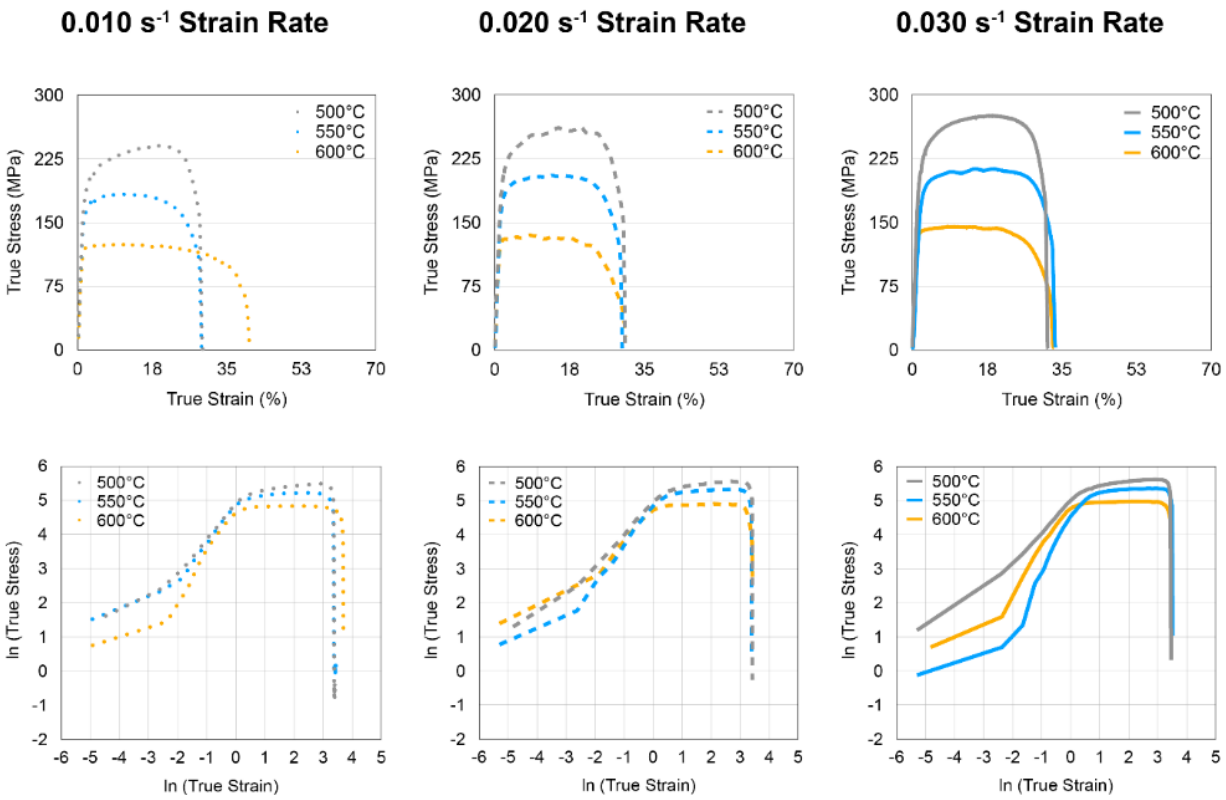

Figure 12 Hot tensile testing results of the weld (A36-A36) specimens.

The power-law was considered to evaluate the creep behaviors, as written in Equation 1.

$$\sigma = k\varepsilon^n \quad (1)$$

where σ is the flow stress, k is the material constant, ε is the true strain, and n is the strain-hardening exponent. The values of n can be determined from the slope of the log-log scale of the true stress - true strain curves. The values of k are the values of true stress at $\varepsilon = 1$. The calculated n and k values are listed in Tables 5 and 6.

Table 5 The n and k values calculated from the hot tensile tests of the Base (A36) specimens

Strain Rates (s^{-1})	Temperature (°C)	n	k
0.002	500	0.166	5.093
0.002	550	0.015	4.955
0.002	600	0.006	4.607
0.002	650	0.007	4.133
0.010	500	0.112	5.200
0.010	550	0.059	5.040
0.010	600	0.024	4.808
0.010	650	0.011	4.357
0.020	500	0.101	5.331
0.020	550	0.025	5.284
0.020	600	0.045	4.850
0.020	650	0.005	4.556

Table 6 The n and k values calculated from the hot tensile tests of the weld (A36-A36) specimens

Strain Rates (s^{-1})	Temperature (°C)	n	k
0.010	500	0.077	5.260
0.010	550	0.032	5.131
0.010	600	0.000	4.811
0.020	500	0.070	5.363
0.020	550	0.030	5.240
0.020	600	0.001	4.882
0.030	500	0.082	5.393
0.030	550	0.039	5.246
0.030	600	0.014	4.940

According to the true stress - true strain curves, the Base (A36) and weld (A36-A36) strengths decreased with increasing temperatures. The results are considered typical for steel materials at elevated temperatures. By taking the true stress at tensile strength values mapped with different strain rates, as presented in Figure 13, the strain hardening effects were very similar for both base and weld specimens. Thus, the overall hot tensile testing results indicated that the A36-A36 weld could be operated under high temperatures. In other words, the lowest strength areas were mainly in the BZ because their large grain sizes were highly influenced by the temperatures (distorted or curved at both BZ ends). The implication of this analysis meant that the areas prone to failure at high temperatures would be the BZ close to HAZ.

The scanning electron microscopic (SEM) images of both base and weld specimens are shown in Figure 14. The necking locations and cross-section images at break indicated that both base and weld specimens' failure mode was a ductile fracture. Particularly on the weld specimens, the necking areas only occurred in the BZ close to HAZ, which agreed with the aforementioned weakest points.

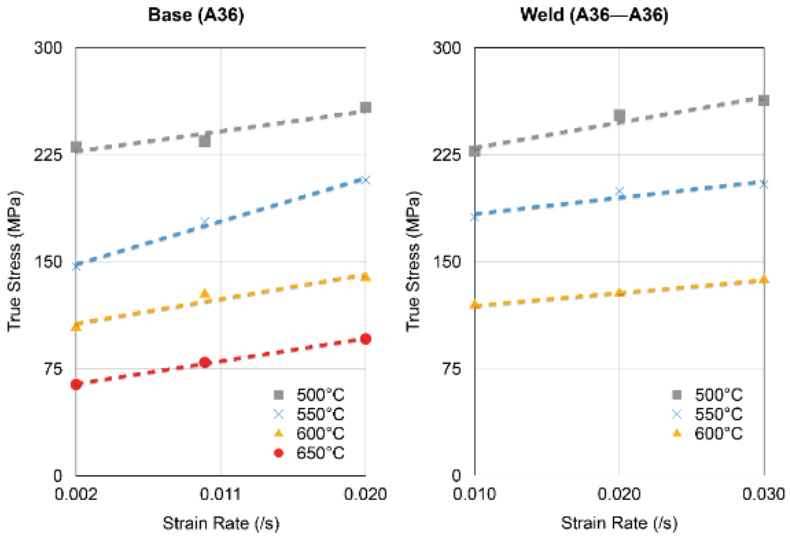

Figure 13 The true stress at tensile strength vs. strain rate of the tested specimens.

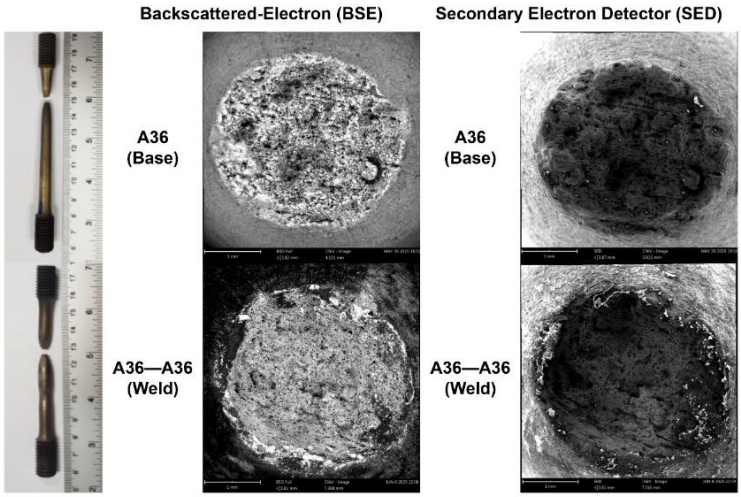

Figure 14 Scanning electron microscopic (SEM) images of the tested specimens.

4. Discussion

By comparing the creep results obtained from our work to the other studies, the tensile strengths of both the base and weld specimens of this work were in the same range as those of the existing work on non-weld low carbon steels [29, 30]. The agreed results implied that the A36-A36 welded plates' strengths would not be inferior to the base plate. The BZ' microstructures were mainly large grain sizes, which had lower strengths (hardness values) than those of the HAZ and WFZ. Although the residual stress results showed that the A36-A36 welded plates were acceptable, the areas that must be paid attention to at high temperatures was the BZ close to HAZ because these were the locations prone to ductile fracture. The results analysis also indicated that the welding process did not significantly affect the A36-A36 weld fusion zone. The n and k values calculated from the hot tensile tests of the A36-A36 welded plates could also be used to estimate the operating conditions under creep. The base and weld's strain hardening behaviors depended on the microstructures, which were similar to the conclusion of Zhu and Xuan's work [30]. By observing the fractography (Figure 14), it could be implied that potential void nucleations or ductile dimples would be more pronounced in BZ, leading to the fracture in that area [33, 34]. Based on the A36-A36 welded joints' analyzed creep behaviors, these welded joints could be used to operate at high temperatures. The only main concern that one must consider was the weakest areas in the BZ close to HAZ at elevated temperatures.

5. Conclusions

The mechanical investigations on the welded joints of A36-A36 under creep conditions were presented. The main conclusions are listed as follows:

(1) The base (A36) zones had large grains and lower hardness values than those of the HAZ and weld fusion zones. As a result, the mechanical strengths of the base zones were the lowest.

(2) At elevated temperatures and varied strain rates, the weld metal (A36-A36) zones were not significantly affected by increased temperatures. The base zones were the weakest locations due to their large grains.

(3) Ductile fracture was the failure mode of the A36-A36 welded plates. The areas prone to this type of failure was the base zones close to HAZ.

6. Acknowledgements

This research was funded by the Thailand Research Fund (TRF), grant number PHD5910086. The authors would like to acknowledge the supports of LPN Metallurgical Research Center; Department of Mechanical Engineering, Faculty of Engineering, Khon Kaen University; King Mongkut's University of Technology Thonburi; National Metal and Materials Technology Center (MTEC); and Department of Mechanical Engineering, Northwestern University.

7. References

[1] Fabricius A, Jackson PS. Premature grade 91 failures-worldwide plant operational experiences. Eng Fail Anal. 2016;66:398-406.
[2] Kassner ME. Fundamentals of creep in metals and alloys. 3rd ed. UK: Butterworth-Heinemann; 2015.
[3] Nabarro FRN, Villiers Fd. Physics of creep and creep-resistant alloys. US: CRC Press; 2018.
[4] Creep-Resistant steels. Woodhead publishing series in metals and surface engineering. USA: Woodhead Publishing; 2008.
[5] Abe F. Progress in creep-resistant steels for high efficiency coal-fired power plants. J Pres Ves Tech. 2016;138(4).
[6] Madyira DM, Liebenberg JA, Kaymacki A. Comparative characterization of P91 and 10crmo9-10 creep resistant steel welds. Procedia Manuf. 2017;8:345-52.
[7] Pandey C, Mahapatra MM, Kumar P. Effect of post weld heat treatments on fracture frontier and type IV cracking nature of the crept P91 welded sample. Mater Sci Eng. 2018;731:249-65.
[8] Pandey C, Mahapatra MM, Kumar P, Kumar S, Sirohi S. Effect of post weld heat treatments on microstructure evolution and type IV cracking behavior of the P91 steel welds joint. J Mater Process Tech. 2019;266:140-54.
[9] Pandey C, Mahapatra MM, Kumar P, Vidyrathy RS, Srivastava A. Microstructure-based assessment of creep rupture behavior of cast-forged P91 steel. Mater Sci Eng. 2017;695:291-301.
[10] Pandey C, Mahapatra MM, Kumar P, Saini N. Some studies on P91 steel and their weldments. J Alloy Comp. 2018;743:332-64.
[11] Jovicic R, Sedmak S, Cvetkovic RP, Popovic O, Bubalo KJ, Milosevic N. Effects of welding technology on the occurrence of fracture in welded joints. Procedia Struct Integrity. 2018;13:1682-8.
[12] Zhao L, Jing H, Xu L, Han Y, Xiu J. Experimental study on creep damage evolution process of Type IV cracking in 9Cr-0.5Mo-1.8W-VNb steel welded joint. Eng Fail Anal. 2012;19:22-31.
[13] Sakthivel T, Laha K, Chandravathi KS, Parameswaran P, Tailor HM, Vasudevan M, et al. Integrity assessment of grade 92 welded joint under creep condition. Procedia Eng. 2014;86:215-22.
[14] Wei Y, Qiao S, Lu F, Liu W. Failure transition mechanism in creep rupture of modified casting 9Cr-1.5Mo-1Co welded joint. Mater Des. 2016;97:268-78.
[15] Liu W, Lu F, Wei Y, Ding Y, Wang P, Tang X. Special zone in multi-layer and multi-pass welded metal and its role in the creep behavior of 9Cr1Mo welded joint. Mater Des. 2016;108:195-206.
[16] El-Desoky OE, Abd El-Azim ME, ElKossy MR. Analysis of creep behavior of welded joints of P91 steel at 600 °C. Int J Pres Ves Pip. 2019;171:145-52.
[17] Chaurasia PK, Pandey C, Giri A, Saini N, Mahapatra MM. A comparative study of residual stress and mechanical properties for FSW and TIG weld on structural steel. Arch Metall Mater. 2018;63(2):1019-29.
[18] Taraphdar PK, Thakare JG, Pandey C, Mahapatra MM. Novel residual stress measurement technique to evaluate through thickness residual stress fields. Mater Lett. 2020;277:128347.
[19] Taraphdar PK, Pandey C, Mahapatra MM. Finite element investigation of IGSCC-prone zone in AISI 304L multipass groove welds. Arch Civ Mech Eng. 2020;20(2):54.
[20] Josef B. Creep Mechanics. 3rd ed. Berlin: Springer; 2008.
[21] Rusinko A, Rusinko K. Plasticity and creep of metals. Berlin: Springer; 2011.
[22] Zhao L, Jing H, Xu L, An J, Xiao G. Numerical investigation of factors affecting creep damage accumulation in ASME P92 steel welded joint. Mater Des. 2012;34:566-75.
[23] Prokhorov A, Kostina A, Vedernikova A, Plekhov O, Menaka M, Venkatraman B. Experimental and numerical investigation of the fracture in steel welded joints. Procedia Struct Integrity. 2018;13:1521-6.
[24] Lagoda T. Lifetime estimation of welded joints. Berlin: Springer; 2011.
[25] Besson J, Leclercq S, Gaffard V, Gourgues-Lorenzon AF. Analysis of creep lifetime of an ASME Grade 91 welded pipe. Eng Fract Mech. 2009;76(10):1460-73.
[26] Jelwan J, Chowdhury M, Pearce G. Design for creep: a critical examination of some methods. Eng Fail Anal. 2013;27:350-72.
[27] Wang X, Wang X, Luo B, Guo J. Analysis of cavity evolution in 9%Cr heat-resistant steel welded joint during creep. Eng Fract Mech. 2018;202:394-404.
[28] Zhang W, Wang X, Wang Y, Yu X, Gao Y, Feng Z. Type IV failure in weldment of creep resistant ferritic alloys: II. Creep fracture and lifetime prediction. J Mech Phys Solid. 2020;134:103775.
[29] Kelly FS, Sha W. A comparison of the mechanical properties of fire-resistant and S275 structural steels. J Constructional Steel Res. 1999;50(3):223-33.
[30] Zhu ML, Xuan FZ. Effect of microstructure on strain hardening and strength distributions along a Cr-Ni-Mo-V steel welded joint. Mater Des. 2015;65;707-15.
[31] Pandey C, Mahapatra MM. Effect of groove design and post-weld heat treatment on microstructure and mechanical properties of p91 steel weld. J Mater Eng Perform. 2016;25(7):2761-75.
[32] Pandey C. Mechanical and metallurgical characterization of dissimilar p92/ss304 l welded joints under varying heat treatment regimes. Metall Mater Trans. 2020;51(5):2126-42.
[33] Pandey C, Mahapatra MM, Kumar P, Saini N. Effect of creep phenomena on room-temperature tensile properties of cast & forged P91 steel. Eng Fail Anal. 2017;79:385-96.
[34] Pandey C, Mahapatra MM, Kumar P, Sirohi S. Fracture behavior of crept P91 welded sample for different post weld heat treatments condition. Eng Fail Anal. 2019;95:18-29.